Available online at www.sciencedirect.com
ScienceDirect
Trans. Nonferrous Met. Soc. China 29(2019) 1677−1688
Transactions of Nonferrous Metals Society of China
www.tnmsc.cn

Microstructure and mechanical characterization of Incoloy 825 Ni-based alloy welded to 2507 super duplex stainless steel through dissimilar friction stir welding

Jalal KANGAZIAN, Morteza SHAMANIAN

Department of Materials Engineering, Isfahan University of Technology, Isfahan, 8415683111, Iran

Received 22 November 2018; accepted 29 May 2019

Abstract: The feasibility of dissimilar friction stir welding (FSW) between the SAF 2507 super duplex stainless steel and the Incoloy 825 Ni-based superalloy was evaluated. The microstructure and mechanical behavior of the weldments were examined too. The results showed that the alloys were successfully welded together by positioning the SAF 2507 on the advancing side. The nuggets displayed higher hardness than the base metals, due to the occurrence of dynamic recrystallization and the subsequent refinement of the microstructures. The welded sample obtained the similar strength to the Incoloy 825 parent metal, showing the ductile fracture mode after the tensile tests by SEM. Moreover, the weld zone (31 J) exhibited higher and lower toughness than the Incoloy 825 (23 J) and SAF 2507 (42 J) parent metals, respectively. Based on the obtained results, the FSW method could be recommended to weld the super duplex stainless steel/Ni-based superalloy joints.

Key words: friction stir welding; dissimilar welds; nickel; stainless steel; microstructure; mechanical property

1 Introduction

Duplex (DSS) and super duplex stainless steel (SDSS), as candidates replacing the conventional austenite stainless steel [1], display excellent mechanical and corrosion properties such as high strength, good toughness and good resistance to the pitting and crevice corrosion [2]. Ni-based superalloys are very attractive materials due to such excellent characteristics as perfect combination of good yield, tensile and creep strengths and also, corrosion resistance [3].

Dissimilar welding between stainless steel and Ni-based superalloys have significant advantages in a transition from high temperature sections to moderately high temperature environments [4], e.g., gas turbine engines, geothermal power plant, and chemical processing equipment, as well as oil and gas industry [5−7]. However, it has been reported that one of the most challenging issues in dissimilar welding of these materials, by fusion welding methods, is selection of the suitable filler wire [8]. The use of Ni-based filler metals containing Mo and Nb elements can result in the segregation phenomenon, leading to the formation of brittle intermetallic phases, such as Lave phase and $M_{23}C_6$ and/or MC-type carbides, at room temperature; these, in turn, tend to deteriorate toughness and ductility of the weldments [9]. Moreover, the secondary phases may be performed during or after employing under severe working (high temperature) conditions; for instance, oil-reformer towers can be mentioned [10]. On the other hand, the use of DSS filler wires can result in some susceptibility to the formation of the brittle phase, like chromium nitride (Cr_2N), sigma (σ) and chi (χ) [9]. Also, utilizing the modern fusion welding methods, such as electron beam welding (EBW), has not suppressed the formation of the secondary phases properly [11]. The presence of such phases in the weld metal decreases pitting corrosion resistance and the mechanical behavior of the joints [12,13]. Although some attempts have been made to eliminate these limitations [14], the problem has not been solved completely.

The friction stir welding (FSW) was developed in 1991 by The Welding Institute (TWI) of the United Kingdom as a solid state welding method. This welding process has many advantages such as low distortion of workpiece, no loss of alloying elements, and good dimensional stability, in comparison to the fusion

Corresponding author: Jalal KANGAZIAN; E-mail: j.kangazian@ma.iut.ac.ir
DOI: 10.1016/S1003-6326(19)65074-0

welding methods [15]. It was especially developed for dissimilar and non-dissimilar joining of light weight alloys [16]. But, limited researches have been conducted to develop FSW for the joining of SDSS, DSS and Ni-based superalloys.

SATO et al [17] investigated microstructure and mechanical properties of SAF 2507 SDSS non-dissimilar FS welds. They obtained a high-quality weld using the polycrystalline cubic boron nitride (PCBN) tool and optimum FSW parameters. SAEID et al [18] studied the influence of the welding travel speed on the microstructures and the mechanical behavior of non-dissimilar SAF 2205 DSS. They reported that increasing the welding speed caused a decrease in the size of the austenite and ferrite grains, thereby leading to the improvement of the hardness values. SONG et al addressed FSW process parameters for the non-dissimilar joining of Inconel 600 [19], Inconel 718 [20] and Inconel 625 [21] Ni-based superalloys. BARABASH et al [22] investigated the effect of friction stir processing (FSP) on the cast microstructure of Inconel 738 Ni-based superalloys. They observed that due to the severe plastic deformation during FSP, the dendritic microstructure was completely destroyed and a fine submicron-crystalline microstructure was generated.

Review of the literatures demonstrated that dissimilar FSW between Ni-base superalloy and DSS (or SDSS) has not been attempted yet. Furthermore, limited studies have been done to investigate dissimilar FSW between the stainless steel and Ni-based alloys [23]. Recently, we investigated the microstructure and mechanical properties of Incoloy 825/SAF 2507 SDSS dissimilar welds using fusion welding processes [24]. We found that segregation and/or non-optimal heat input could result in the formation of some deteriorating phases. However, solid state welding methods, especially FSW, could suppress the segregation phenomenon.

The aim of this work was probing the feasibility of the dissimilar FSW between SAF 2507 SDSS and Incoloy 825 Ni-based superalloy and evaluating the microstructures and mechanical properties. It has been reported [25] that Incoloy 825 and SAF 2507 SDSS are structural materials that can be used to build the vessels.

2 Experimental

2.1 Materials and welding

The parent metals employed in this work were the SAF 2507 SDSS and Incoloy 825 Ni-based superalloy with the dimensions of 100 mm × 50 mm × 3 mm. The chemical composition of the base metals is listed in Table 1. Before welding, a square joint design was prepared and the base metals were cleaned mechanically and chemically using SiC papers and some acetone solution to remove contaminations such as rust. The welding tool was made of a WC-based alloy with the shoulder diameter of 18 mm, the pin diameter of 5 mm and the pin length of 2.8 mm. Also, the tool was tilted about 3° from the plate normal direction during welding. Four samples were welded in different rotational speeds, travel speeds and the base metals positioning, as given in Table 2.

The welding direction was perpendicular to the rolling direction of base metals in all samples. The schematic view of the FSW process and its tool is represented in Fig. 1. The heat inputs for the samples were calculated according to the following equation [16]:

$$Q=4\eta\mu PWR^3\pi^2/(3V) \quad (1)$$

where Q is the heat input per unit weld length, η is the heat input efficiency, μ is the friction coefficient, P is the pressure due to the tool plunge down force, W is the rotational speed, V is the travel speed, and R is the radius of the shoulder. The axial force (about 14 kN) was considered to be the fixed parameter. In addition, all parameters (except W and V) in Eq. (1) were assumed to be constant (about 7.9 [18]) for the joints; thus, the heat inputs were calculated, as given in Table 2.

Table 1 Chemical composition of base metals (wt.%)

Material	C	Cr	Ni	Si	Mn	Ti	N	Mo	Cu	Fe
Incoloy 825	0.01	22.05	Bal.	−	0.72	0.64	−	3.28	2.18	31.28
SAF 2507	0.03	25.70	6.30	0.93	0.82	−	0.23	3.40	−	Bal.

Table 2 Process parameters employed in dissimilar FSW

Sample No.	Travel speed, V/(mm·min^{-1})	Rotational speed, W/(r·min^{-1})	Advancing side (AS)	Retreating side (RS)	Depth of penetration/mm	Heat input/ (J·mm^{-1})
1	40	700	Incoloy 825	SAF 2507	2.8	138.25
2	40	1000	Incoloy 825	SAF 2507	2.8	197.50
3	24	1000	Incoloy 825	SAF 2507	2.8	329.16
4	40	700	SAF 2507	Incoloy 825	2.8	138.25

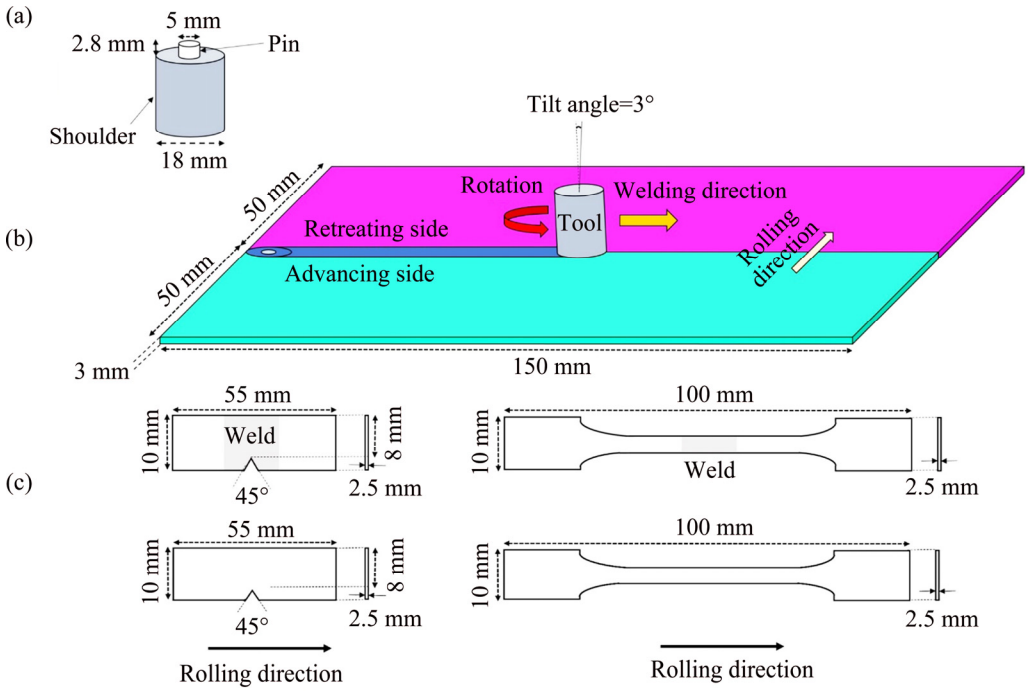

Fig. 1 Schematic views of tool (a), friction stir welding (b) and transverse tensile test and Charpy test samples of parent metals and sample No. 4 (c)

2.2 Microstructural characterizations

After welding, the samples were cut from the weldments. Then, the cross sections of the samples were mounted by epoxy resin, ground on SiC paper from 80 to 1200 grit, and polished by alumina suspension (0.05 μm in particle size). The specimens were etched using an electrolytic method with 10% oxalic acid and 6 V power supply. Optical microscopy (OM), scanning electron microscopy (SEM) equipped with an energy-dispersive X-ray spectroscopy (EDS), and X-ray diffraction analysis (XRD) with Cu K_α (λ=0.154 nm) radiation were used. A HITACHI SU8230 field emission SEM was employed for electron backscattered scattering detection analysis of the weld zone (step size of 1.5 μm). The electron backscatter diffraction (EBSD) map was undertaken by the channel 5 software.

2.3 Mechanical tests

In order to evaluate the mechanical behavior of weldments, three mechanical tests including micro-hardness, tensile and V-notch Charpy impact toughness tests were conducted. In the micro-hardness test, a Vickers pyramid indenter with a load of 300 g and time of 10 s was employed on the transverse section of the weldment. Tensile samples were cut in accordance with ASTM: E8/8M (sub-sized sample: 100 mm × 10 mm × 2.5 mm), and the tests were conducted with 2 mm/min cross-head velocity. V-notch Charpy samples were cut from the weld zone according to ASTM: E23-12c (sub-sized sample: 55 mm × 10 mm × 2.5 mm; 45° V-notch at the weld metal) and the impact tests were conducted at room temperature. The schematic view of the tensile and Charpy test samples is depicted in Fig. 1. All mechanical tests were repeated at least three times to ensure the reproducibility of the data. After tensile and impact tests, the fracture surfaces of the samples were examined using SEM.

3 Results and discussion

3.1 Appearance of welds

There are some investigations addressing FSW parameters for DSS [18,26] and Ni-based alloys [19]. In these works, the primary parameters were distinguished and Incoloy 825 was selected as the advancing side (AS). According to Fig. 1, the direction of the tool transverse speed and rotation speed was the same at AS; however, the opposite side was named the retreating side (RS). Figure 2 shows the joint appearance and the cross section of the primary samples. Sample No. 1 as the first sample was fabricated by the tool rotation speed and travel speed of 700 r/min and 40 mm/min, respectively. Figure 2(a) depicts the crack on surface of the stir zone (SZ) and the formation of a defect known as “tunnel”-like defect at AS (Incoloy 825). According to the literature, formation of the void or the tunnel-shaped defect during dissimilar FSW at AS could be due to the high welding speed (insufficient heat input), insufficient forging pressure, and a too large joint cap [27].

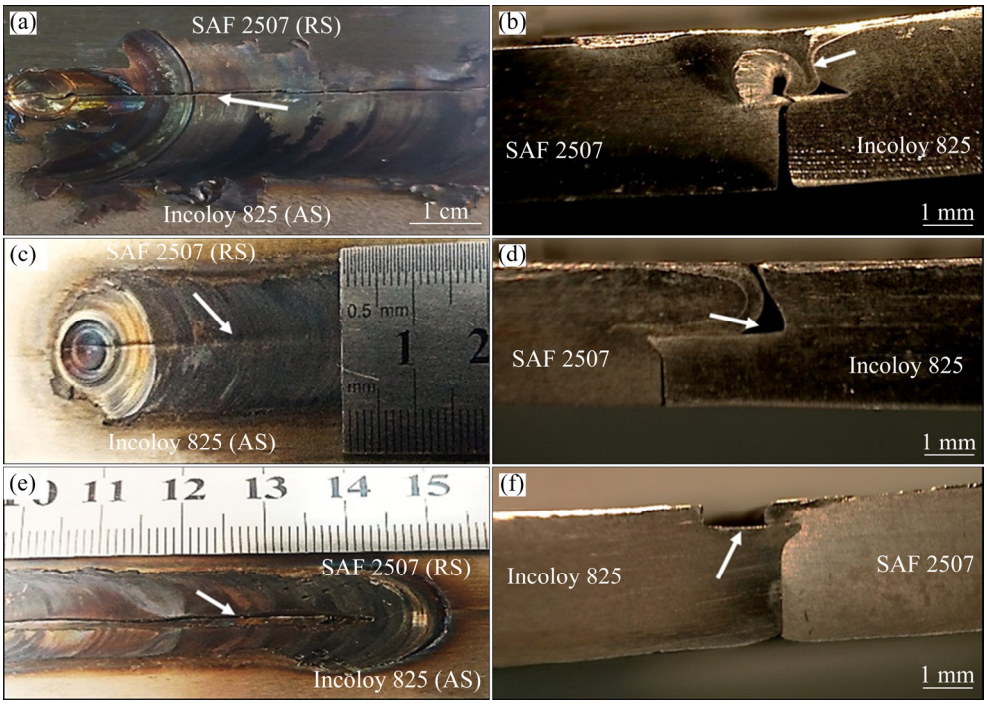

Fig. 2 Macrostructures of samples: (a, b) No. 1; (c, d) No. 2; (e, f) No. 3; (a, c, e) Surface; (b, d, f) Cross section (RS: Retreating side, AS: Advancing side)

The heat input of FSW process could be increased by raising the tool rotation speed and/or decreasing the tool travel speed based on Eq. (1) and Arbegast−Hartley equation, as represented below [16]:

$$T_p/T_m=K(W^2/10000V)^{\alpha} \quad (2)$$

where K is a constant in the range of 0.65−0.75, α is between 0.04 and 0.06, T_m is the melting point of the alloy, and T_p is the maximum temperature during welding. Equation (2) demonstrates that T_p and thus, heat input could be increased by decreasing V and/or enhancing W. Therefore, the rotational speed was increased to 1000 r/min for the No. 2 sample; then the travel speed was decreased to 24 mm/min for the No. 3 sample. The heat inputs for the samples are also presented in Table 2. However, according to Figs. 2(c, d) and 2(e, f), the cracks and tunnel defects were not eliminated. Then, SAF 2507 was positioned on the AS, and 700 r/min and 40 mm/min FSW parameters (No. 4 sample) were employed. It should be noted that the tool wear occurred in all experiments.

The surface appearance and the cross section of No. 4 are presented in Fig. 3. The No. 4 sample did not display any conventional defects such as voids, tunnel shape, and crack. The materials were completely mixed with each other. The macroscopic examination (Fig. 3(a)) divulged that the interface between the two alloys did not show the sharpness feature and the vortex-like material flow was dominant. The sharp interfaces are usually

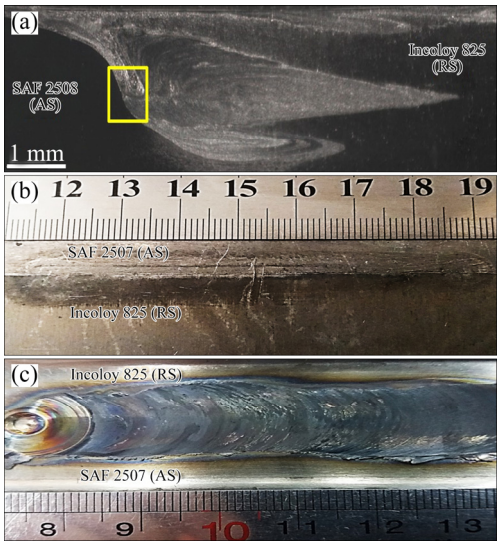

Fig. 3 Macrostructures of sample No. 4: (a) Cross section; (b) Back; (c) Surface of weldment (RS: Retreating side, AS: Advancing side)

presented in a zigzag shape and formed in the lower heat input; they can also be observed in the dissimilar welding between the alloys with a large difference in flow stress at the welding temperature, such as Al to steel or Al to Ti [28]. This macro-interface is formed due to the insufficient heat input which permits good stirring and intermixing of both alloys, resulting in the lower weld strength [28]. It could be seen that positioning the material having the higher strength and flow stress (SAF 2507), as compared to the other case (Incoloy 825),

on the AS could result in some weld having the acceptable quality. However, positioning the Incoloy 825 on the AS could result in the void and tunnel defect formation. It could be attributed to the asymmetrical stress and the strain between AS and RS during the FSW process [29].

It has been reported [16] that AS, when being compared to the RS, generates a higher strain. Positioning the material having higher flow stress on the AS could lead to the formation of some kind of balance between material flows from the front to the back of the pin during FSW [29]. In other words, the asymmetric nature of the process would be compensated by the suitable arrangement of the dissimilar material. Positioning the Incoloy 825 (with the lower flow stress) on the AS could lead to the higher material flow in front of the tool, as compared to the back, during the progress of the tool; thus, void formation was dominant at AS. The results were in a good agreement with the previous researches [23,30].

3.2 Microstructure

Figures 4 and 5 show the microstructure of the joint for the No. 4 sample. It can be seen that the “onion ring” shape was formed in AS; also, AS was sharper than the RS. Formation of the onion ring is usual at the FSW of Al alloys [16]; it has also observed in the weld of Mg/Al alloys [31] and stainless steels [32].

The cross section of the weldment for each alloy was divided to three distinct regions containing the base metal, the thermo-mechanical affected zone (TMAZ) and the nugget or SZ. It is worth mentioning that the

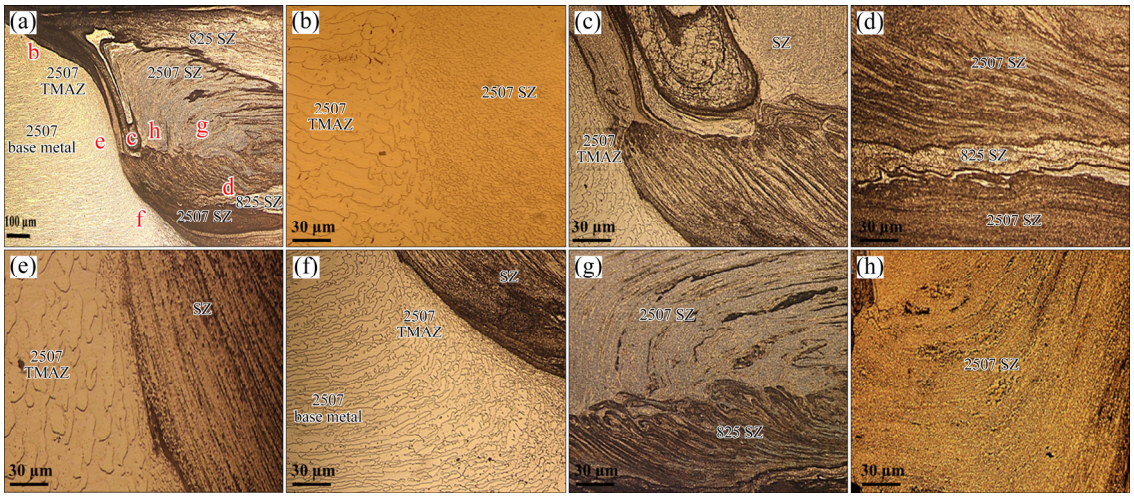

Fig. 4 Optical microstructures of No. 4 sample cross section at SAF 2507 side: (a) Weld zone; (b−h) Areas marked in (a) (SZ: Stir zone, TMAZ: Thermo-mechanical affected zone)

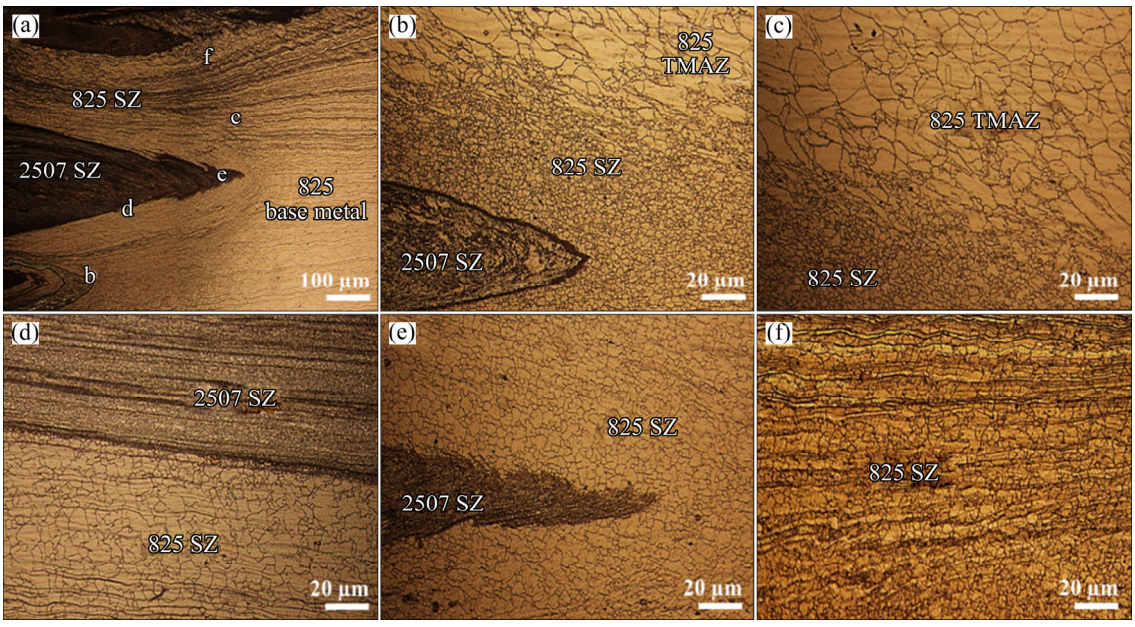

Fig. 5 Optical microstructures of No. 4 sample cross section at Incoloy 825 side: (a) Weld zone; (b−f) Areas marked in (a) (SZ: Stir zone, TMAZ: Thermo-mechanical affected zone)

heat-affected zone (HAZ) was not observed clearly for both alloys. Other researchers have not observed the HAZ clearly after the FSW of DSS [18] and Ni-based alloys [21]. This could be attributed to the combination of the fast cooling rate during welding and the natural feature (physical properties) of the parent metals.

The microstructure of the base metals is represented in Fig. 6. Incoloy 825 is the solid-solution-strengthened Ni-based superalloy. This alloy has a fully equiaxed austenitic microstructure. Some cubic, dispersed, secondary phases could be observed in the matrix as Ti(N,C) phases. These phases have also been characterized in the previous research [33]. The austenite phase in the ferrite matrix, as the elongated form, was observed in SAF 2507 SDSS. It could be seen that the secondary phase was not detected. TMAZ at the SAF 2507 side (Fig. 4) was the region distinguished by shifting the grains from the rolling direction, rather than the base metal. In other words, the elongated grains of the parent metal were deformed. This was due to the strain (experienced during FSW) and/or the limited recrystallization phenomenon that occurred in TMAZ [34]. Such a microstructure has also been previously observed in the TMAZ of SDSS or DSS [30,35].

In order to better investigate TMAZ at SAF 2507 SDSS, the phase map of the selected (rectangular) area in Fig. 3(a) has been described in Fig. 7. This phase map

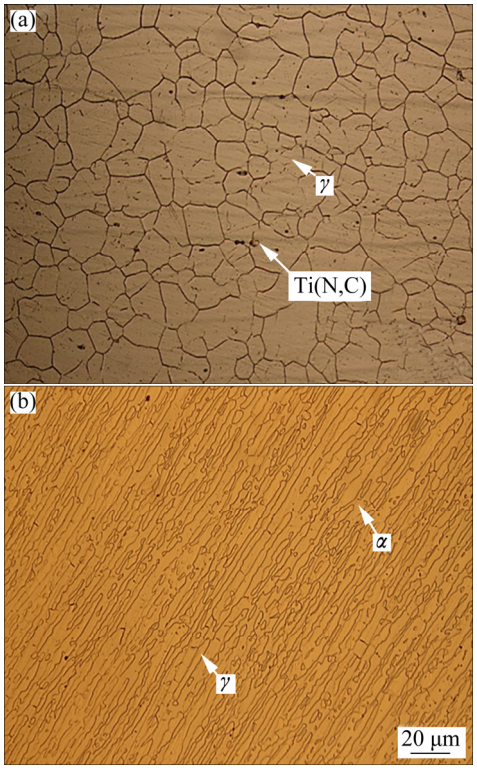

Fig. 6 Microstructures of base metals: (a) Incoloy 825; (b) SAF 2507

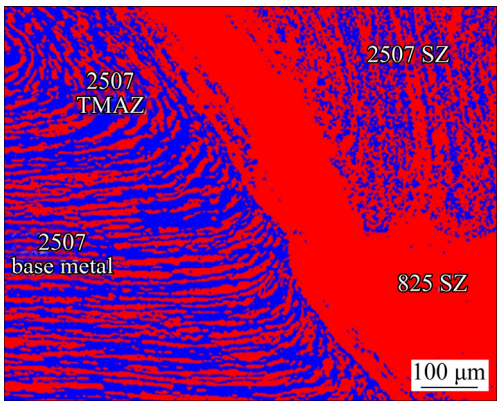

Fig. 7 Phase map micrograph at rectangular area indicated in Fig. 3(a) (Red color: Austenite phase, Blue color: Ferrite phase, SZ: Stir zone, TMAZ: Thermo-mechanical affected zone)

shows that austenite (red color area) and ferrite (blue color area) phases were deformed adjacent to the SZ. The elongated grains were shifted and thus, the sharp feature was generated at AS. The microstructure of the TMAZ at the Incoloy 825 side is presented in Fig. 5. In this region, the elongated austenite and the twining boundaries were observed. Moreover, some fine grain austenite was observed in the grain boundaries adjacent to the SZ. Experiencing the combination of exposure at high temperature and a high strain could lead to the formation of the elongated austenite, twining boundary and limited recrystallization. It is well accepted that the dynamic recrystallization (DRX) phenomenon occurs in SZ [16]. This phenomenon refines the microstructure, especially grain size, thereby resulting in the generation of finer grains.

The SZ at the SAF 2507 side has finer ferrite–austenite grains (Figs. 4 and 5) than the original base metal (Fig. 6). It has been reported that during the FSW of SDSS, ferrite (as the high stacking fault energy (SFE) phase) and austenite (as the low SFE phase) phases undergo continuous dynamic recrystallization (CDRX) and discontinuous dynamic recrystallization (DDRX) mechanisms, respectively [17]. Microstructural investigations have demonstrated that the austenite grains are finer than the ferrite grains. In other words, the equiaxed austenitic islands distribute in the ferrite matrix. Formation of the finer grains of austenite, as compare to those of the ferrite, could be attributed to the higher stability of ferrite, rather than austenite, at the higher temperatures [18].

In DSS and/or SDSS, austenite to ferrite transformation is realized by heating. This transformation is completed at about 1327 °C [36] and at the higher temperature (up to the solidus temperature), the microstructure contains the fully ferrite phase. In this study, although thermal profiles were not measured by

thermocouple, previous works have shown that the FSW peak temperature at the DSS plates is varied from (about) 700 to 1000 °C based on the FSW parameters employed [18,26]. Moreover, according to Eq. (2), the calculated peak temperature at the SZ of 2507 side was estimated to be about 954 °C. Therefore, SZ of SAF 2507 could be heated up to the ferrite−austenite phase region (not the ferrite single phase region).

Heating the SDSS and/or DSS at the ferrite single-phase region (above 1250 °C) resulted in the formation of more ferrite phase (austenite to ferrite transformation). After subsequent fast cooling from the ferrite single-phase region, precipitation of secondary phases, such as chromium nitride, could occur at the SZ, or ferrite to austenite ration balance would be changed (far from 1:1 ratio), in comparison with the DSS parent metal [37]. Formation of the brittle phase and/or unbalanced ferrite to austenite ratio could deteriorate the mechanical and corrosion behavior of DSS [12,38].

Figure 8 displays the X-ray diffraction pattern of SZ. The results demonstrated that the secondary phases were not formed and/or the contents were lower than the limit of detection determined by XRD (lower than about 5%). Also, investigation of SZ by SEM did not show any secondary phases at the cross section of the weldment. SANTOS et al [35] studied the FSW of UNS S32101 and S32205 DSS, and S32750 and S32760 SDSS alloys. They observed some secondary phase (sigma and/or chromium nitride phase) only in the SZ of S32760 SDSS. On the other hand, the SZ of Incoloy 825 side, as shown in Fig. 5, only contained the fully fine grain austenite. Due to experiencing the high temperature and high strain, austenite phase underwent the DRX phenomenon.

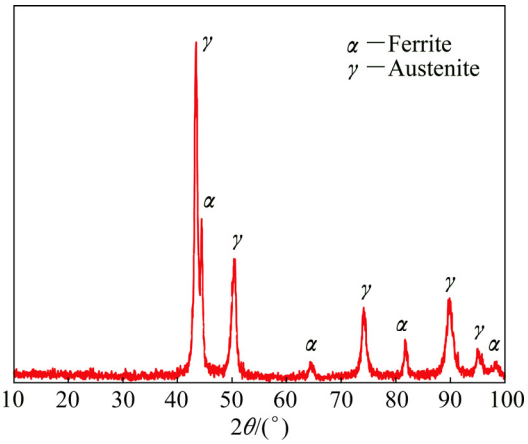

Fig. 8 X-ray diffraction pattern of SZ in No. 4 weld metal

These results were in a good agreement with previous researches observing the refinement of austenite in the SZ of the Ni-based alloy, such as Inconel 718 [20], Inconel 625 [21] and Inconel 600 [19]. As mentioned above, the austenite phase has a relatively low SFE; thus, it could undergo the DDRX mechanism during the FSW process. Similar to the SZ of SAF 2507, the investigations by SEM and the obtained X-ray diffraction pattern in Fig. 8 did not reveal the formation of any secondary phase. Based on Eq. (2), the peak temperature would be estimated to be about 980 °C in the SZ of Incoloy 825. SONG et al [19] and LIPPOLD et al [39] reported that the peak temperature during the FSW and the FSP of some Ni-based alloys varied from 670 to 890 °C and from 850 to 1100 °C, respectively.

According to Figs. 4 and 5, Incoloy 825 flowed to the top and bottom of the SZ of SAF 2507 SDSS. The flow patterns of SAF 2507 could also be observed in Figs. 4 and 5. Moreover, the phase map micrograph (Fig. 7) demonstrated that Incoloy 825 shifted to the AS near the SZ/TMAZ boundary. The material flow during the FSW of Incoloy 825 to 2507 SDSS welds would lead to the formation of the boundary between both SZs.

Figure 9 represents the interface formed between the SZs. The SEM photographs and line scan analysis showed that the secondary phases were not formed. Furthermore, EDS point analysis (Fig. 10) demonstrated that the interface had 37.99 wt.% Ni, similar to the

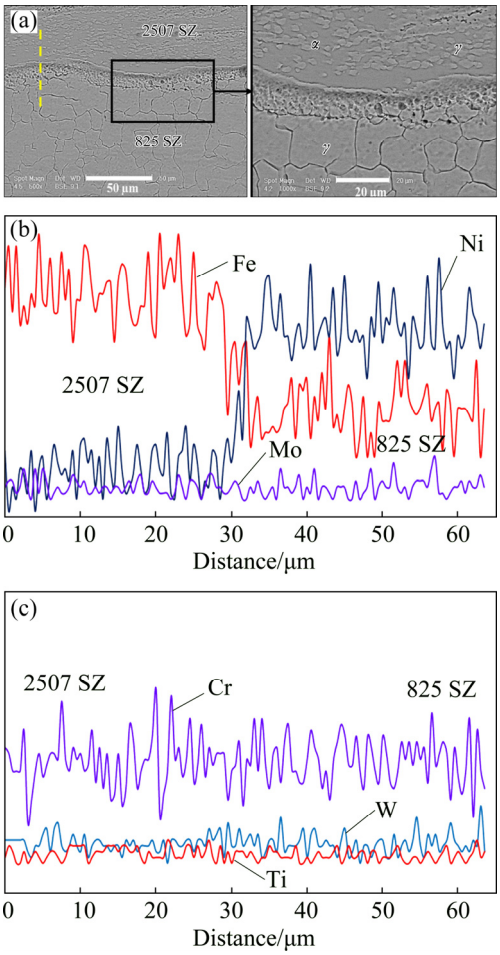

Fig. 9 SEM micrograph of interface of stir zones (a), and line scan analysis results across line (b, c) (SZ: Stir zone)

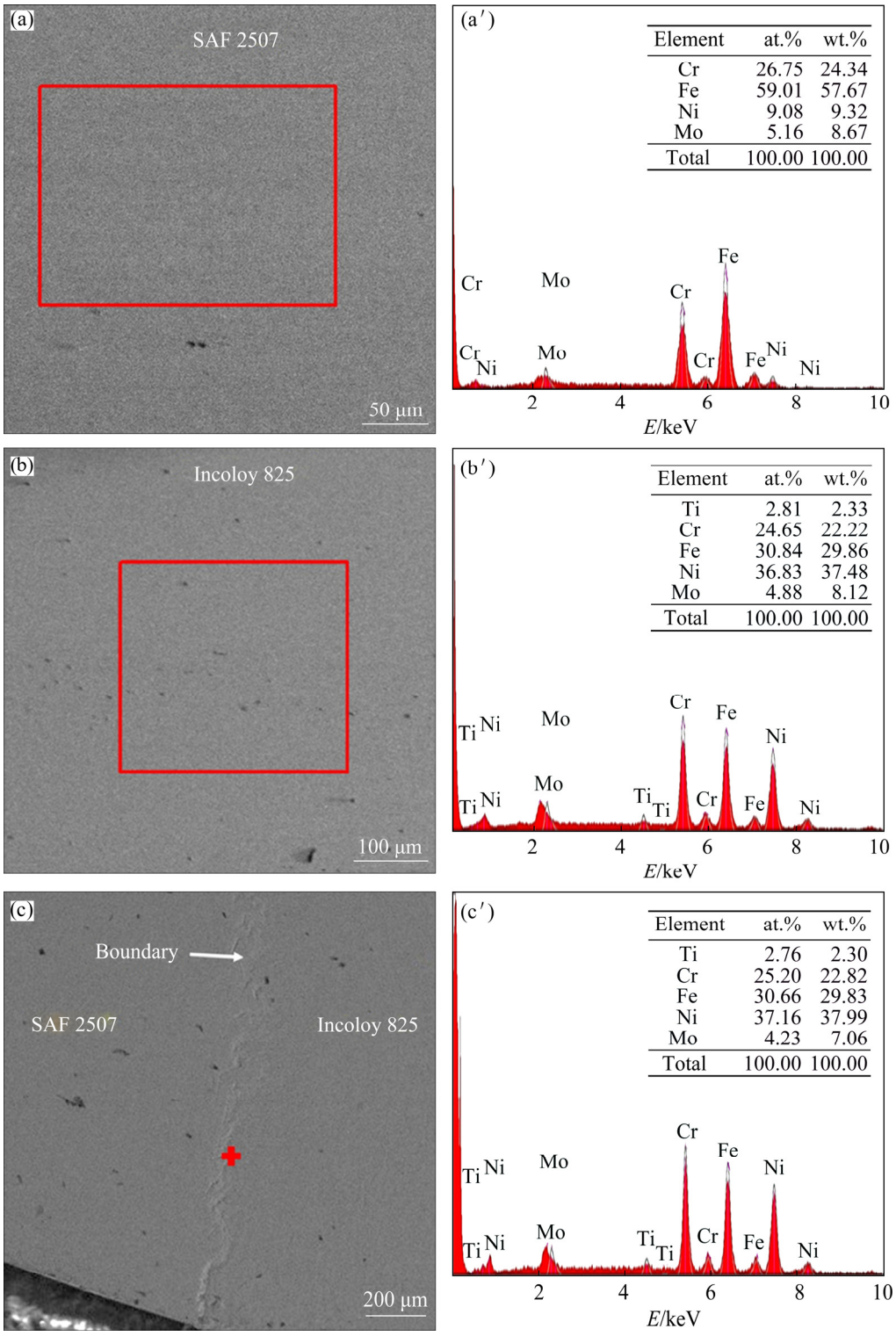

Fig. 10 EDS analysis results at stir zone of SAF 2507 (a, a′), Incoloy 825 (b, b′), and interface (c, c′)

Incoloy 825 (37.48 wt.% Ni). In other words, the chemical composition of the interface was similar to the Incoloy 825. It has been reported that the dissimilar FSW between the alloys with the high affinity to each other, such as Al to Mg, could result in the formation of the secondary or intermetallic phases that would decrease the joint quality and the properties [31].

The line scan analysis of the W element showed that although some fluctuations observed in the line scan corresponded to the agglomeration of the W element, the distribution of the W element was generally uniform in the SZs. The line scan showed that a W-rich band structure and serious agglomeration of the W element were not formed in the SZs. SONG and NAKATA [20]

observed a W-rich band structure in the SZ of Inconel 718 due to the serious wear of the W-based tool during FSW. The W-rich debris entrapped within the SZs could prevent sound metallurgical bonding, leading to the deterioration of tensile properties of the weldments [40].

3.3 Mechanical properties

Micro-hardness, tensile and impact toughness tests were conducted to evaluate the mechanical behavior of the No. 4 weldment. It is worth mentioning that No. 1, No. 2 and No. 3 samples had some defects, as mentioned above, and therefore, mechanical properties of the defect-free sample (No. 4) were only studied. The micro-hardness profile at the cross section of the No. 4 sample is shown in Fig. 11(a).

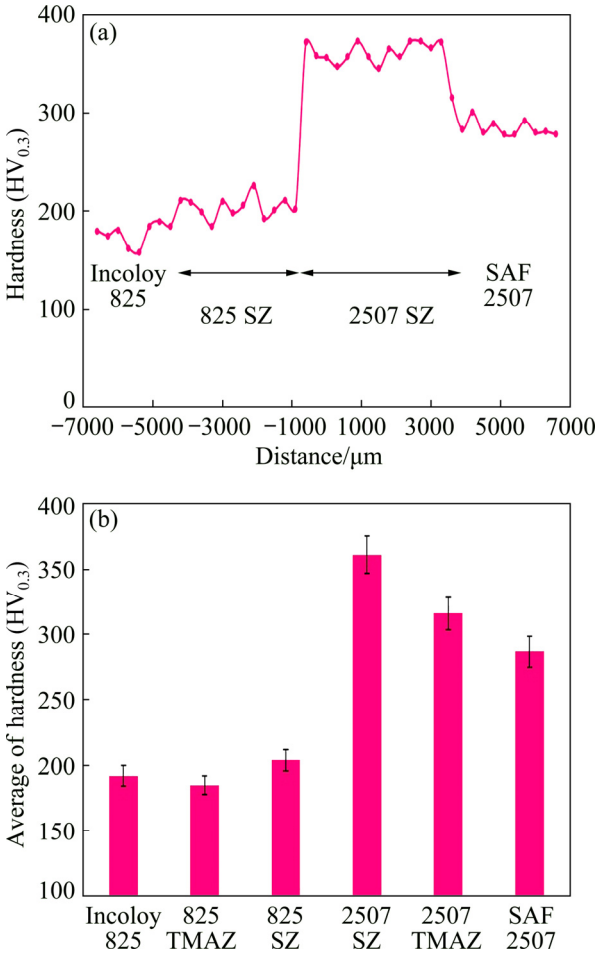

Fig. 11 Micro-hardness profiles at cross section of No. 4 sample (a) and average hardness values (b) (SZ: Stir zone, TMAZ: Thermo-mechanical affected zone)

The average micro-hardness of each area is presented in Fig. 11(b). It could be seen that, the hardness distribution was asymmetrical. The hardness values were increased from the Incoloy 825 base metal (192 HV) and TMAZ (185 HV) to the SZ of Incoloy 825 (204 HV). On the other hand, the hardness values were increased from the SAF 2507 base metal (287 HV) to TMAZ (317 HV) and then, the SZ of 2507 SDSS (361 HV). This showed that each SZ had significantly higher hardness values than the relative parent metal. The higher micro-hardness of SZ could be attributed to the refinement of the microstructure during the FSW process, due to the RX phenomenon. According to the well-known Hall–Petch relationship [18], decreasing the grain size could result in the enhancement of strength and the hardness. The results agreed with those reported by LI et al [41].

Figure 12 shows the engineering stress−strain curves of the base metal and the No. 4 sample. The data extracted from Fig. 12 are presented in Table 3. Based on the data, SAF 2507 SDSS showed the highest yield strength (654 MPa) and tensile strength (877 MPa). The yield and tensile strengths of No. 4 sample were similar to those of the Incoloy 825 parent metal. This revealed that the weld metal displayed the suitable strength during the transverse tensile test. But the elongation of the weldment (12%) was lower than that of the SAF 2507 (23%) and Incoloy 825 (48%). The elongation reduction should be attributed to the incompatible deformation between two dissimilar materials during the tensile test. Before the fracture of the Incoloy 825, the SAF 2507 hardly yields. Thus, the deformation mainly occurs on Incoloy 825, and the elongation decreases [41]. Other researchers [42,43] have also reported that FS weldments show lower elongation than the parent metal(s).

Figure 13 demonstrates that during the tensile tests,

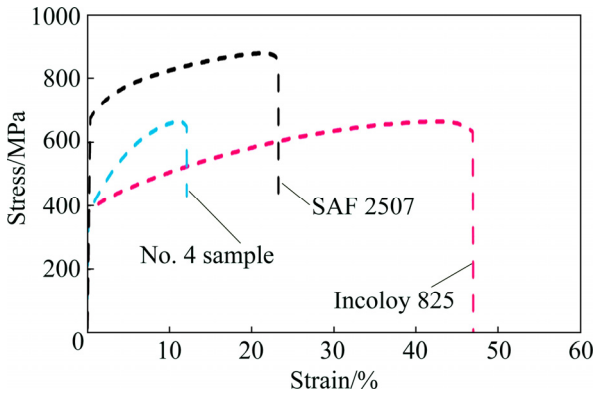

Fig. 12 Engineering stress−strain curves of base metals and No. 4 sample

Table 3 Mechanical properties of No. 4 sample and parent metals

Mechanical property	No. 4 sample	Base metal	
		SAF 2507	Incoloy 825
Tensile strength/MPa	685±10	877±15	653±20
Yield strength/MPa	391±10	654±15	375±16
Elongation/%	12±2	23±2	48±3
Impact toughness/J	31±2	42±3	23±3

although fracture occurred from the RS, the crack was not propagated through the interfaces of the materials. It was shown that the alloys were completely mixed with each other; thus, the interface did not act as the weaker site. The occurrence of the fracture from RS could be attributed to the curvature of the weldment surface. During welding, due to the pressure of the tool (especially shoulder) on the surface of the plates, plastic deformation could result in curvature on the surfaces. The patterns of such deformation are represented in Figs. 4 and 5. Incoloy 825 (as RS) had lower yield strength than SAF 2507, according to the data shown in Table 3; therefore, it experienced higher plastic deformation than the other case. The curvature of the surface could generate the stress concentration. Hence, it would produce the preferential fracture site at RS. Furthermore, examination of the fractured surface after the tensile test (Fig. 14(a)) revealed that the ductile mode of the fracture was dominant. The formation of void, micro-void and dimples, as the fracture surface topography, could be clearly observed.

The toughness of the weld joint was investigated by using the impact Charpy testes at room temperature. The impact toughness data are displayed in Table 3. According to the obtained data, the weld metal showed higher impact resistance (31 J) than the Incoloy 825 base metal (23 J). However, the weld metal showed lower impact resistance in comparison with the SAF 2507 base metal (42 J). The weld metal of the sample No. 4 contained the combination of the fine grains of austenite (Incoloy 825) and ferrite–austenite (SAF 2507) microstructures. As can be seen, although the formation of such a structure in the weld metal of the No. 4 sample resulted in the higher impact resistance than the Incoloy 825 base metal, it caused lower toughness compared to the SAF 2507 parent metal. The SAF 2507 represented the highest toughness due to the presence of a dual phase microstructure. RAHMANI et al [44] observed that SDSS base metal displayed higher impact resistance than the (single-phase) austenitic stainless steel. It is well-known that a nearly balanced ferrite to austenite ratio (1:1) in DSS or SDSS alloys could lead to the improvement of mechanical properties, especially impact resistance [44,45]. Although grain refinement at SZs could be regarded as a reason for the improvement of impact property, the weld metal of the No. 4 sample had two different alloys mixed with each other, leading to the formation of inhomogeneous microstructures. Hence, the lower impact toughness of the weld zone, rather than the SAF 2507 base metal, could be attributed to the presence of inhomogeneous microstructures and incompatible deformation between these two dissimilar materials during FSW. The fractured surface of No. 4 sample after the impact test (Fig. 14(b)) revealed the formation of dimples and voids; thus, the ductile mode of the fracture was dominant.

To summarize, this study addressed the feasibility of the dissimilar FSW between SAF 2507 SDSS and Incoloy 825 Ni-based superalloy. The effects of FSW parameters on the quality of the welds were investigated. The microstructure and mechanical properties of the high quality weldment were characterized. The influence of the tool rotation speed, the tool travel speed, and the axial force on the microstructure, mechanical properties, and the corrosion behavior of the dissimilar welds was left for future works.

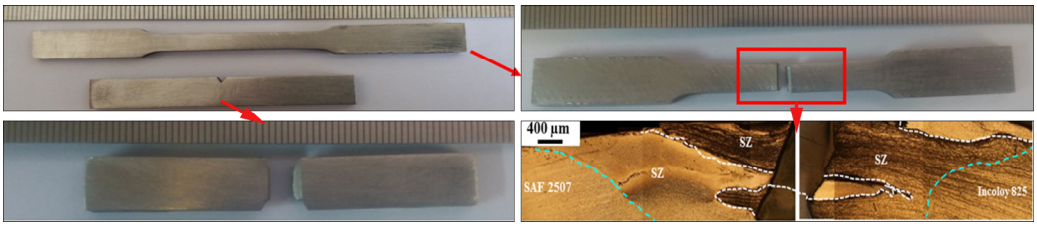

Fig. 13 Appearance of tensile and impact samples prior and after tests (SZ: Stir zone)

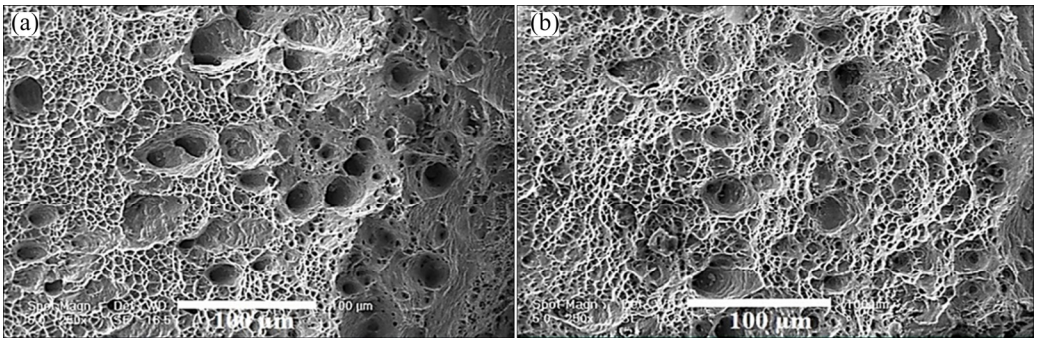

Fig. 14 SEM fractographs of tensile (a) and impact (b) samples

4 Conclusions

(1) Macroscopic observations demonstrated that positioning the Incoloy 825 on the advancing side did not result in the formation of sound welds. However, the defect-free joint was obtained by positioning the SAF 2507 on the advancing side.

(2) Microstructural analysis indicated that the heat affected zone was not observed at both base metals. The thermo-mechanical affected zone was characterized as the elongated austenite at the Incoloy 825 side and deformed austenite−ferrite grains at the SAF 2507 side.

(3) According to tensile tests, the yield and tensile strengths of the sample fabricated by positioning the SAF 2507 on the advancing side were similar to those of Incoloy 825 parent metal. The fratograghy results revealed that the ductile fracture mode was dominant.

(4) The results of impact toughness tests demonstrated that the weld zone obtained higher impact resistance than the Incoloy 825 parent metal and lower toughness, as compared to the SAF 2507 base metal. The welded sample underwent the ductile mode of fracture during the impact test.

References

[1] LUO H, DONG C F, XIAO K, LI X G. Characterization of passive film on 2205 duplex stainless steel in sodium thiosulphate solution [J]. Applied Surface Science, 2011, 258: 631−639.

[2] GENG S, SUN J, GUO L, WANG H. Evolution of microstructure and corrosion behavior in 2205 duplex stainless steel GTA-welding joint [J]. Journal of Manufacturing Processes, 2015, 19: 32−37.

[3] ZHANG P, QIANG Z, GANG C, QIN H Y, WANG C J. Grain size based low cycle fatigue life prediction model for nickel-based superalloy [J]. Transactions of Nonferrous Metals Society of China, 2018, 28: 2102−2106.

[4] PAVAN A H V, VIKRANT K S N, RAVIBHARATH R, SINGH K. Development and evaluation of SUS 304H-IN 617 welds for advanced ultra supercritical boiler applications [J]. Materials Science and Engineering A, 2015, 642: 32−41.

[5] XU X Y, MA X D, WONG H, YE Z, CHANG J W, XU Y, SUN G A, LU W J, GAO Y K. Characterization of residual stresses and microstructural features in an Inconel 718 forged compressor disc [J]. Transactions of Nonferrous Metals Society of China, 2019, 29: 569−578.

[6] RAMKUMAR K D, SRIDHAR R, PERIWAL S, OZA S, SAXENA V, HIDAD P, ARIVAZHAGAN N. Investigations on the structure–property relationships of electron beam welded Inconel 625 and UNS 32205 [J]. Materials and Design, 2015, 68: 158−166.

[7] HERNANDEZ M, AMBRIZ R R, CORTES R, GOMORA C M, PLASCENCIA G, JARAMILLO D. Assessment of gas tungsten arc welding thermal cycles on Inconel 718 alloy [J]. Transactions of Nonferrous Metals Society of China, 2019, 29: 579−587.

[8] NAFFAKH H, SHAMANIAN M, ASHRAFIZADEH F. Dissimilar welding of AISI 310 austenitic stainless steel to nickel-based alloy Inconel 657 [J]. Journal of Materials Processing Technology, 2008, 9: 3628−3639.

[9] RAMKUMAR K D, CHANDRASEKHAR A, SRIVASTAVA A, PREYAS H, CHANDRA S, DEV S, ARIVAZHAGAN N. Effects of filler metals on the segregation, mechanical properties and hot corrosion behaviour of pulsed current gas tungsten arc welded super-austenitic stainless steel [J]. Journal of Manufacturing Processes, 2016, 24: 46−61.

[10] NAFFAKH H, SHAMANIAN M, ASHRAFIZADEH F. Influence of artificial aging on microstructure and mechanical properties of dissimilar welds between 310 stainless steel and Inconel 657 [J]. Metallurgical and Materials Transactions A, 2008, 39: 2403−2415.

[11] LEE H T, LIN Y D. Microstructure and corrosion behaviour of alloy 690−SUS 304L butt joints formed by electron beam welding [J]. Science and Technology of Welding and Joining, 2006, 11: 650−656.

[12] YOUSEFIEH M, SHAMANIAN M, SAATCHI A. Influence of heat input in pulsed current GTAW process on microstructure and corrosion resistance of duplex stainless steel welds [J]. Journal of Iron and Steel Research International, 2011, 18: 65−69.

[13] YOUSEFIEH M, SHAMANIAN M, SAATCHI A. Optimization of the pulsed current gas tungsten arc welding (PCGTAW) parameters for corrosion resistance of super duplex stainless steel (UNS S32760) welds using the Taguchi method [J]. Journal of Alloys and Compound, 2011, 509: 782−788.

[14] SILVA C C, AFONSO C R M, RAMIREZ A J, MOTTA M F, MIRANDA C, FARIAS J P. Assessment of microstructure of alloy Inconel 686 dissimilar weld claddings [J]. Journal of Alloys and Compound, 2016, 684: 628−642.

[15] WAHID M A, SIDDIQUEE A N. Review on underwater friction stir welding: A variant of friction stir welding with great potential of improving joint properties [J]. Transactions of Nonferrous Metals Society of China, 2018, 28: 193−219.

[16] MISHRA R S, MA Z Y. Friction stir welding and processing [J]. Materials Science and Engineering R: Reports, 2005, 50: 1−78.

[17] SATO Y S, NELSON T W, STERLING C J, STEEL R J, PETTERSSON C. Microstructure and mechanical properties of friction stir welded SAF 2507 super duplex stainless steel [J]. Materials Science and Engineering A, 2005, 397: 376−384.

[18] SAEID T, ABDOLLAH-ZADEH A, ASSADI H, MALEK-GHAINI F. Effect of friction stir welding speed on the microstructure and mechanical properties of a duplex stainless steel [J]. Materials Science and Engineering A, 2008, 496: 262−268.

[19] SONG K H, FUJII H, NAKATA K. Effect of welding speed on microstructural and mechanical properties of friction stir welded Inconel 600 [J]. Materials and Design, 2009, 30: 3972−3978.

[20] SONG K H, NAKATA K. Microstructural and mechanical properties of friction-stir-welded and post-heat-treated Inconel 718 alloy [J]. Journal of Alloys and Compounds, 2010, 505: 144−150.

[21] SONG K H, NAKATA K. Effect of precipitation on post-heat-treated Inconel 625 alloy after friction stir welding [J]. Materials and Design, 2010, 31: 2942−2947.

[22] BARABASH O M, BARABASH R I, ICE G E, FENG Z, GANDY D. X-ray microdiffraction and EBSD study of FSP induced structural/phase transitions in a Ni-based superalloy [J]. Materials Science and Engineering A, 2009, 524: 10−19.

[23] AGHAEI A, DEHGHANI K. Characterizations of friction stir welding of dissimilar Monel 400 and stainless steel 316 [J]. The International Journal of Advance Manufacturing Technology, 2015, 77: 573−579.

[24] KANGAZIAN J, SHAMANIAN M. Characterization of structure–property relationship of Incoloy 825 and SAF 2507 dissimilar welds [J]. Transactions of the Indian Institute of Metals, 2018, 71: 1747−1757.

[25] LINTON V M, LAYCOCK N J, THOMSEN S T, KLUMPERS A. Failure of a super duplex stainless steel reaction vessel [J]. Engineering Failure Analysis, 2004, 11: 243−256.

[26] ESMAILZADEH M, SHAMANIAN M, KERMANPUR A, SAEID

T. Microstructure and mechanical properties of friction stir welded lean duplex stainless steel [J]. Materials Science and Engineering A, 2013, 561: 486−491.
[27] RODRIGUEZ J, RAMIREZ A J. Friction stir welding of mild steel to alloy 625–Development of welding parameters [J]. Science and Technology of Welding and Joining, 2014, 19: 343−349.
[28] SIMAR A, AVETTAND-FÈNOËL M N. State of the art about dissimilar metal friction stir welding [J]. Science and Technology of Welding Joining, 2016, 22: 389−403.
[29] RODRIGUEZ J, RAMIREZ A J. Microstructural characterisation of friction stir welding joints of mild steel to Ni-based alloy 625 [J]. Materials Characterization, 2015, 110: 126−135.
[30] THEODORO M C, PEREIRA V F, MEI R R, RAMIREZ A J. Dissimilar friction stir welding between UNS S31603 austenitic stainless steel and UNS S32750 superduplex stainless steel [J]. Metallurgical Materials Transactions B, 2015, 46: 1440−1447.
[31] AZIZIEH M, ALAVIJEH A S, ABBASI M, BALAK Z, KIM H S. Mechanical properties and microstructural evaluation of AA1100 to AZ31 dissimilar friction stir welds [J]. Materials Chemistry and Physics, 2016, 170: 251−260.
[32] LI H, YANG S, ZHANG S, ZHANG B, JIANG Z, FENG H, HAN P, LI J. Microstructure evolution and mechanical properties of friction stir welding super-austenitic stainless steel S32654 [J]. Materials and Design, 2017, 118: 207−217.
[33] BUSCH J D, DEBARBADILLO J J, KRANE M J M. Flux Entrapment and titanium nitride defects in electroslag remelting of Incoloy alloys 800 and 825 [J]. Metallurgical and Materials Transactions A, 2013, 44: 5295−5303.
[34] LIPPOLD J C. Welding metallurgy and weldability [M]. New Jersey: John Wiley & Sons, 2015.
[35] SANTOS T F A, TORRES E A, LIPPOLD J C, RAMIREZ A J. Detailed microstructural characterization and restoration mechanisms of duplex and superduplex stainless steel friction-stir-welded joints [J]. Journal of Materials Engineering and Performance, 2016, 25: 5173−5188.
[36] LIPPOLD J C, KOTECKI D J. Welding metallurgy and weldability of stainless steels [M]. New Jersey: John Wiley Hoboken, 2005.
[37] NAGHIZADEH M, MOAYED M H. Investigation of the effect of solution annealing temperature on critical pitting temperature of 2205 duplex stainless steel by measuring pit solution chemistry [J]. Corrosion Science, 2015, 94: 179−189.
[38] GHOLAMI M, HOSEINPOOR M, MOAYED M H. A statistical study on the effect of annealing temperature on pitting corrosion resistance of 2205 duplex stainless steel [J]. Corrosion Science, 2015, 94: 156−164.
[39] LIPPOLD J C, RODELAS J M, RULE J R. Friction stir processing of Ni-base alloys [C]//Proceedings of the 1st International Joint Symposium on Joining and Welding. Woodhead Publishing, 2013: 369−376.
[40] MISHRA R S, DE P S, KUMAR N. Friction stir welding and processing: Science and engineering [M]. Springer, 2014.
[41] LI H B, JIANG Z H, FENG H, ZHANG S C, LI L, HAN P D, MISRA R D, LI J Z. Microstructure, mechanical and corrosion properties of friction stir welded high nitrogen nickel-free austenitic stainless steel [J]. Materials and Design, 2015, 84: 291−299.
[42] KARAMI S, JAFARIAN H, EIVANI A R, KHEIRANDISH S. Engineering tensile properties by controlling welding parameters and microstructure in a mild steel processed by friction stir welding [J]. Materials Science and Engineering A, 2016, 670: 68−74.
[43] ESMAEILI A, GIVI M K B, RAJANI H R Z. A metallurgical and mechanical study on dissimilar friction stir welding of aluminum 1050 to brass (CuZn30) [J]. Materials Science and Engineering A, 2011, 528: 7093−7102.
[44] RAHMANI M, EGHLIMI A, SHAMANIAN M. Evaluation of microstructure and mechanical properties in dissimilar austenitic/ super duplex stainless steel joint [J]. Journal of Materials Engineering and Performance, 2014, 23: 3745−3753.
[45] MOTESHAKKER A, DANAEE I, MOEINIFAR S, ASHRAFI A. Hardness and tensile properties of dissimilar welds joints between SAF 2205 and AISI 316L [J]. Science and Technology of Welding and Joining, 2016, 21: 1−10.

异种搅拌摩擦焊 Incoloy 825 镍基超合金和 2507 超级双相不锈钢的显微组织和力学性能

Jalal KANGAZIAN, Morteza SHAMANIAN

Department of Materials Engineering, Isfahan University of Technology, Isfahan, 8415683111, Iran

摘　要：研究 SAF 2507 超级双相不锈钢和 Incoloy 825 镍基超合金间使用异种搅拌摩擦焊(FSW)的可行性，检测焊缝的显微组织和力学行为。结果表明，通过将 SAF 2507 定位在前进侧，可以将两种合金成功焊接在一起。由于熔核发生动态再结晶，以及熔核显微结构的细化，熔核的硬度高于基体硬度；所得焊接样品具有与 Incoloy 825 母合金相近的强度；SEM 观察拉伸测试后的样品显示，其断裂模式为韧性断裂，焊缝区的断裂韧性(31 J)比 Incoloy 825 母合金的(23 J)高，而比 SAF 2507 母合金的(42 J)低。 基于以上结果可知，FSW 方法适用于焊接超级双相不锈钢/镍基超级合金接头。

关键词：搅拌摩擦焊；异种焊接件；镍；不锈钢；显微组织；力学性能

(Edited by Bing YANG)